TECHNICAL MEMORANDUM

192

Impact of a simple vertical diffusion scheme and of the optimisation time interval on optimal unstable structures

R.Buizza

Research Department

February 1993

European Centre for Medium-Range Weather Forecasts
Europäisches Zentrum für mittelfristige Wettervorhersage
Centre européen pour les prévisions météorologiques à moyen

ABSTRACT

Ensemble forecast prediction is based on the study of an ensemble of time integrations, computed with slightly different initial conditions. Perturbations are superimposed on a basic state to provide a representation of the uncertainty of the initial state of the atmospheric flow. One way to define these perturbations is by computing the fastest growing structures over a finite time interval. The computation of the fastest growing perturbation over a finite time interval can be achieved using the forward and adjoint tangent version of the full non-linear model.

Numerical experiments have been performed to study the impact on the most unstable perturbations of surface drag and a vertical diffusion scheme. A similarity index has been defined to compare the unstable sub-spaces of different experiments. Results show how a very simple parametrization of the turbulent processes avoid non-meteorological structures to grow close to the surface.

The impact of the optimisation time interval, over which perturbation growth has been maximized, on the definition of the unstable sub-space has been studied for time intervals up to three days. Results from different cases indicate that unstable sub-spaces computed with an optimisation time interval longer than 36 hours are very similar. The impact of changing the basic state computation on the unstable sub-space has also been studied.

1. INTRODUCTION

The fastest growing perturbations of a primitive equation model, growing over a finite time interval, can be computed using the adjoint technique first proposed by *Lorenz* (1965). This technique uses the tangent and the adjoint of the tangent version of the full non-linear model to define the most unstable directions in the phase space of the system. A necessary condition for the tangent approximation to be correct is that the perturbations remain small compared to the basic state. Since we are interested in the time evolution of perturbations that represent initial errors, this condition is satisfied with sufficiently small initial errors.

Lacarra and Talagrand (1988) and *Rabier and Courtier* (1991) showed that the time evolution of small perturbations can be described by its linear approximation, if the time interval is not longer than 2-3 days. All our experiments are performed over time periods not longer than 3 days.

After describing briefly the adjoint technique, section 2 describes the simple parametrization of surface drag and turbulent vertical diffusion. A comparison of the non-linear time evolution computed with the simple scheme, with non-linear evolution computed with a version of the ECMWF (European Centre for Medium-Range Weather Forecasts) scheme, is described. In section 3 we study the sensitivity of the most unstable perturbations to the simple physics scheme. The impact of the way the non-linear basic state evolution is computed on the definition of the unstable sub-space is studied in section 4. In section 5 the sensitivity of the definition of the unstable sub-space to the time interval over which the growth has been maximized is studied. Finally, some conclusions are drawn.

1.1 The adjoint technique

Let χ be the state vector in the phase space of the system. The non-linear, primitive equations that describe the time evolution of the system can be formally written in the following way:

$$\frac{d\chi}{dt} = A\chi \tag{1}$$

Let us consider a small perturbation, and let us study its evolution. For sufficiently small time intervals and initial amplitudes, its growth is almost linear, and the problem can be studied in the linear approximation. The model equations 1 can be linearized around the trajectory computed from 1. This gives the linearized equations for the perturbation x:

$$\frac{dx}{dt} = A_l x \tag{2}$$

where A_l is the tangent operator that corresponds to the model operator A.

Let us denote by $L=L(t_0,t)$ the tangent propagator, computed from 2. The perturbation $x(t)$ at time t is given by:

$$x(t) = L\,x(t_0) \tag{3}$$

Let us define an inner product on the space of the perturbations:

$$(x;y) = \langle x;E\,y \rangle \tag{4}$$

where E defines some weighting factors, and where <..;..> is the canonical Euclidean scalar product. We can also define the associated norm of a generic vector:

$$\| x \|^2 = (x;x) = \langle x;E\,x \rangle \tag{5}$$

The norm of the perturbation at time t can be computed using the adjoint of the operator L defined with respect to the inner product 4:

$$\|x(t)\|^2 = (L\,x_0;L\,x_0) = \left(L^{*E}\cdot L\,x_0;x_0\right) \tag{6}$$

The square roots of the eigenvalues of the matrix $L^{*E}\cdot L$ are called the singular values of the matrix L. The eigenvectors of the matrix $L^{*E}\cdot L$ are called the singular vectors of L (hereafter SVs). Since $L^{*E}\cdot L$ is self-adjoint, the SVs are orthogonal. The norm of a SV $v_i(t)$ at time t is given by:

$$\|v_i(t)\|^2 = \left(L^{*E}\cdot Lv_i(t_0);v_i(t_0)\right) = \sigma_i^2 \| v_i(t_0) \|^2 \tag{7}$$

The SVs v_i constitute an orthogonal base of the phase space of the system. They are orthogonal at time t_0 and at the final time t, and their norm at time t can be computed from their initial norm using 6. The singular values σ_i give the amplification factors between t_0 and t for each of them. The directions characterized by the largest singular values are the directions that grow fastest with respect to the norm 5. The computation of the fastest growing perturbations is thus reduced to an eigenvalue problem of the operator $L^{*E}\cdot L$.

A Lanczos algorithm (*Strang*, 1986), developed by the Numerical Algorithm Group (NAG, Oxford, see *Simon*, 1984 for references) has been implemented to solve the eigenvalue problem. The Lanczos algorithm is a very useful technique when a few of the extreme eigenvectors are needed. It can be applied to large and sparse problems. The algorithm does not access directly the matrix elements of the operator that define the problem, but throughout successive applications of the operator it gives an estimate of the eigenvectors. More details on the adjoint technique are described in *Buizza* (1992) and in *Buizza et al.* (1992).

The primitive equation model used for these experiments is the Integrated Forecasting System (IFS): this model is the result of a collaboration between ECMWF and Météo France. The model equations are

described in *Courtier et al.* (1991). It has been used at horizontal triangular truncation T21, with 19 vertical levels (hereafter T21L19). At the time of these experiments the forward and adjoint tangent versions of the adiabatic part with a horizontal diffusion scheme were available. A simple vertical diffusion and surface drag scheme is the first step of a project in which the tangent and the adjoint versions of the diabatic processes will be introduced.

During all the experiments, the T21L19 IFS tangent integration has been carried out following the trajectory computed by the same model, except when explicitly mentioned.

The four situations studied in this paper were chosen after the work of *Molteni and Palmer* (1992) and *Mureau et al.* (1992), and are characterized by regime transitions occurring over a period of 7 days. All the experiments described in sections 2, 3 and 4 have starting date 17.01.89, at 12 UTC. The initial state is characterized by a zonal flow throughout the entire hemisphere, that evolves into a blocked situation over Europe. The sensitivity studies on the impact of the optimisation time interval, described in section 5, have also been done for three other cases. The 17.01.90 initial state is characterized by a blocked flow over north-east Pacific, decaying to give a more zonal circulation after 2 days. The 17.01.91 initial situation is characterized by strong blocking structures developing both over Europe and north-eastern Pacific. The 19.02.91 initial state is characterized by a strongly blocked situation over Europe, that decays after two days to a less blocked situation.

2. IMPACT OF A SIMPLE VERTICAL DIFFUSION SCHEME ON THE BASIC STATE EVOLUTION

In the first part of this section the simple physics scheme implemented is described. In the second part results from three experiments are presented: a control experiment expA run with a version of the operational ECMWF vertical diffusion and surface drag scheme (see ECMWF research manual 3 for references), experiment expB1 with the simple physics, and expC without any scheme. All these experiments have been run with nonlinear normal mode initialization applied to the first 5 gravest modes in the computation of the trajectory, and its linear approximation in the integration of the tangent model.

The simplified parametrization scheme simulates the surface drag and the vertical transport of momentum due to turbulent exchange. The vertical diffusion part of the scheme can be applied also to the dry static energy. The scheme is very simple, essentially for two reasons: the first is a technical reason related to the fact that the trajectory when integrating the tangent and the adjoint version of the model, is available only at the current time (time t). A tangent version of a non-linear scheme, with an implicit time integration, needs the availability of the trajectory at the previous time step. This explains the reason why the scheme has constant coefficients. The second reason is that, before implementing a more complex scheme, we want

to quantify the impact of a basic simulation of the physical process on the most unstable perturbations. Once this has been studied, a more sophisticated scheme can be implemented, if necessary.

In this section we present some results of the impact of the scheme on the basic state non-linear evolution: we want to check if the impact is positive, and we want to quantify the differences in the basic state evolution generated by this scheme compared to the time evolution computed using a version of the operational ECMWF scheme. In section 3 we will study the impact on the unstable structures.

2.1 The linear vertical diffusion and surface drag scheme

The vertical diffusion equation reads:

$$\frac{\partial \psi}{\partial t} = -\frac{\partial F_\psi}{\rho \partial z} \tag{8}$$

In the parametrization of the flux F_ψ we distinguish between the surface layer and the upper layer.

The surface flux of dry static energy is zero, and the surface drag is:

$$F_u = \rho_0 u_* \frac{k U_{19}}{\ln\left(\frac{z_{19}}{z_0}\right)} \quad F_v = \rho_0 u_* \frac{k V_{19}}{\ln\left(\frac{z_{19}}{z_0}\right)} \tag{9}$$

where U_{19}, V_{19} are the velocity components at the lowest model level, and z_{19} is the height above the surface of the lowest model level.

The flux in the upper layer of any variable $\psi = U_x, U_y, S$, where $S = Cp\ T + \phi$ is the static energy, is:

$$F_\psi = \rho_0 u_* l_{diff} f\left(\frac{z}{z_0}\right) \frac{\partial \psi}{\partial z} \tag{10}$$

where the mixing length is defined as:

$$l_{diff} = \frac{k z}{1 + \frac{k z}{\lambda}} \tag{11}$$

The function $f\left(\frac{z}{h_0}\right)$ has been introduced to smoothly decrease the vertical diffusion:

$$f\left(\frac{z}{h_0}\right) = \exp\left(-\frac{z}{h_0}\right) \tag{12}$$

A similar expression, namely $\left(1 - \frac{z}{h_0}\right)^2$, has been proposed by *Troen and Mahrt* (1986). The exponential form turns out to give a smoother result, particularly when a fixed value for h_0 is used.

The finite difference approximation of the vertical diffusion equation, for each grid point, is:

$$\frac{\psi^{t+dt} - \psi^{t-dt}}{2\,dt} = \underline{K}^t \cdot \psi^{t+dt} \tag{13}$$

where $\underline{K}$ is a tridiagonal matrix defined by the surface drag and the vertical diffusion coefficients, and where $\psi = (\psi_1, \psi_2, \ldots, \psi_K)^T$ represents a state vector at grid point (i,j).

The wind velocity scale factor u_* and the roughness length z_0 are functions of the land-sea contrast:

$$u_* = u_*^{\,l}\, LSM + u_*^{\,s}\,(1 - LSM) \tag{14a}$$

$$z_0 = z_0^{\,l}\, LSM + z_0^{\,s}\,(1 - LSM) \tag{14b}$$

where $LSM = 1$ for model land points and $LSM = 0$ for sea points.

2.2 Impact of the scheme on the basic state evolution

The basic state evolutions computed in three different configurations are compared: expA, the control, run with a version of the operational ECMWF scheme, expB1 run with the simple scheme, and expC run without any physical process simulated. ExpB1 was run with the vertical diffusion and the surface drag applied only to the momentum equations, with parameters:

$$u^*_{L\,(S)} = 0.5\ (0.2)\ ms^{-1}$$

$$z_{0_{L\,(S)}} = 0.05\ (0.0005)\ m$$

$$h_0 = 1000\ m$$

Fig. 1 shows the ratio of the kinetic energy at different forecast time with the kinetic energy at the initial time, for the control experiment expA (dashed curved) and expB1 (solid line). The ratio is given in the abscissa, and the number of the model level is given in the ordinate. Three forecast times are shown: 24, 48 and 72 hours. Fig. 2 shows again the control expA, compared with expC run without any physics scheme.

It is clear from the comparison of the two figures that running without the scheme produces a strong wind in the lowest model levels. The application of the simple scheme reduces the generation of winds, with an effect very similar to the effect of a more complex scheme, although differences can be detected. Fig. 3

shows the initial condition, and the 24 h forecast computed by the control expA: the streamfunction at the last three model levels is shown. The difference between the 24 h forecast computed by expB1 and expC, and the control expA (streamfunction), is shown in Fig. 4. Table 1 reports the ratio (in percent) between the differences of the streamfunction field predicted by an experiment and the control, at forecast time t, and the field variation over the 24 h period computed by the control:

$$\epsilon(t) = 100 \frac{<(\psi_i(t)-\psi_A(t))^2>_{mean}}{<(\psi_A(t)-\psi_A(t_0))^2>_{mean}} \tag{15}$$

where $i = B, C$, and where the mean value is computed over all the grid points.

Table 1

Experiment	Level	$\epsilon(t-24h)$	$\epsilon(t-48h)$	$\epsilon(t-72h)$
B1 (C)	15	20 (33)	21 (56)	80 (88)
B1 (C)	17	50 (132)	39 (116)	96 (190)
B1 (C)	18	40 (240)	100 (122)	43 (272)
B1 (C)	19	44 (347)	39 (191)	90 (264)

Table 2 reports the same ratio computed for the temperature field.

Table 2

Experiment	Level	$\epsilon(t-24h)$	$\epsilon(t-48h)$	$\epsilon(t-72h)$
B1 (C)	15	37 (39)	36 (42)	81 (83)
B1 (C)	17	90 (91)	97 (99)	101 (104)
B1 (C)	18	117 (125)	129 (131)	113 (138)
B1 (C)	19	140 (163)	177 (194)	139 (223)

Table 1 shows that the difference between the streamfunction fields of expA and expB1 is small in the lowest model levels, while the difference between expA and expC is very large, confirming the results of Fig. 1. The ratio $\epsilon(t)$ decreases with the model level number: its value relative to the comparison between expA and expB1 is always smaller than 20% for all model levels above level 13 during the first 48 hours. The comparison between the values of expB1 and expC shows that the presence of the simple physics improves the description of the low level flow.

Large differences can be detected when comparing the temperature fields of the two experiments expA and expB1. This could be due to the absence of a turbulent transport of dry static energy. We decided not to apply the vertical diffusion scheme to the dry static energy because of the absence of a scheme to parametrize the surface heat flux. The downward turbulent heat transport to the lowest model levels causes strong warming in the first model levels, and this has a measurable impact on the wind flow. The differences in the temperature field between an experiment run with the vertical diffusion scheme applied also to the dry static energy and expA, were larger than the differences expC-expA.

Some other experiments have been run to test the impact of changing the values of the parameters $u^*_{L,S}$, $z_{0_{L,S}}$, h_0, and to tune them so that the simple scheme was able to give a basic state evolution similar to expA. A small impact on the results was shown by changing the value of the velocity scales and of the roughness lengths by a factor of 2, and the value of the reference height in the range $700\ m \leq h_0 \leq 1500\ m$. The expB1 configuration seems to give the best results.

The comparison of the performances of the two scheme is not the aim of this work; what is important for our purpose is that the scheme gives a reasonable non-linear time evolution during the first 48 hours of integration, and this seems to be the case from the results presented. These results clearly show that computing the basic state evolution without a surface drag and a vertical diffusion scheme produces a very unrealistic flow pattern at the lowest model levels.

3. SVs SENSITIVITY TO A SIMPLE VERTICAL DIFFUSION SCHEME

In this section we compares the SVs structures generated by different experiments performed over a 24 h time interval:

Experiment	Momentum surf drag	Momentum vert diff	Static En vert diff
expB1	yes	yes	no
expB2	yes	yes	yes
expB3	yes	no	no
expC	no	no	no

The SVs have been computed using the Lanczos algorithm: 100 iterations were sufficient to have about 30 SVs with an acceptable accuracy. This implies 100 forward and 100 backward integrations (*Buizza*, 1992 for more details). All the experiments have been performed with the first 5 gravest vertical modes initialized.

The comparison of expB1 and expC shows the impact of the simple physics scheme on the unstable structures. The rationale for expB2 and expB3 is to quantify the impact on the SVs of the surface drag and the vertical diffusion. The comparison expB1-expB3 gives the impact of the turbulent momentum transport, when the surface drag in applied to the horizontal momentum equations, while the comparison expB2-expB1 permits us to study the impact of the application of the turbulent transport to the dry static energy. Other experiments have been run to check the sensitivity of the SVs to the tuning parameters $u^*_{L,S}$, $z_{0_{L,S}}$, h_0: we will briefly comment on this below.

We define the ***N-dim*** unstable sub-space relative to an experiment as the sub-space of the phase space of the system defined by the first N most unstable perturbations. We can compare the unstable sub-spaces generated by the first N SVs v_i of two experiments A and B using a projection matrix $M(A,B;N)$, defined using the scalar product definition 1.4, as:

$$m_{i,j}(A,B) = \left(\langle v_i(A);E\ v_j(B)\rangle\right)^2 \tag{16}$$

Each element of this matrix is the squared scalar product between the i-th SV of the A experiment, and the j-th SV of the B experiment. In other words, it represents the amount of the energy of the i-th SV of the A experiment that is explained by the j-th SV of the B experiment. The sum of the matrix elements with a fixed first index represents how the well the i-th SV of the A experiment can be reconstructed from a linear combination of the first N SVs of the B experiment.

We define a similarity index of two experiments A,B, that measures the similarity of the unstable sub-spaces generated by the first N SVs of each experiment, as:

$$s\ (A,B;N) = \frac{1}{N}\sum_{i,j=1}^{N} m_{i,j}\ (A,B) \tag{17}$$

Table 3 gives the projection matrix $M\ (B1,C;20)$, computed with N=20, for expB1, the experiment run with the physics scheme applied to the momentum components, and expC run without any physical parametrization scheme. Differences can be detected; if we consider the definition of the leading unstable directions, we can see that the 2nd, the 6th and the 7th SV of expC are orthogonal to all the first 20 SVs of expB1. These SVs have very large amplitude in the lower model levels: if superimposed on an initial condition field, and integrated using a non-linear model with included physical processes, they rapidly disappear due to the action of the physics parametrization. These structures have a very strong baroclinic structure, with the temperature field changing sign at each model level in the first three model levels. A comparison of the tangent evolution compared to the non-linear T63 evolution of a SV with a similar structure has been shown in *Buizza* (1992). The simple scheme prevents these structures from growing: the

	1	2	3	4	5	6	7	8	9	10	11	12	13	14	15	16	17	18	19	20	
1	99	0	1	0	0	0	0	0	0	0	0	0	0	0	0	0	0	0	0	0	100
2	1	0	98	0	0	0	0	0	0	0	0	0	0	0	0	0	0	0	0	0	99
3	0	0	0	96	0	0	0	0	0	0	0	0	0	0	0	0	0	0	0	0	97
4	0	0	0	0	96	0	0	0	0	0	0	0	0	0	0	0	0	0	0	0	97
5	0	0	0	0	0	0	0	6	1	88	0	0	0	0	0	0	0	0	0	0	97
6	0	0	0	0	0	0	0	1	50	0	46	0	0	0	0	0	0	0	0	0	97
7	0	0	0	0	0	0	2	28	14	1	28	2	1	0	0	0	0	0	0	3	80
8	0	0	0	0	0	0	1	6	11	2	8	54	1	0	2	0	0	0	0	0	87
9	0	0	0	0	0	0	0	0	0	0	0	0	8	0	9	59	16	6	0	0	98
10	0	0	0	0	0	0	0	0	0	0	0	0	69	2	20	0	1	0	0	0	94
11	0	0	0	0	0	0	0	0	0	0	0	0	3	0	28	2	59	1	0	1	94
12	0	0	0	0	0	0	0	0	0	0	0	0	8	0	31	24	18	7	2	1	93
13	0	0	0	0	0	0	0	0	0	0	0	0	0	0	0	0	2	14	66	14	97
14	0	0	0	0	0	0	0	0	0	0	0	0	1	0	2	8	0	49	7	8	75
15	0	0	0	0	0	0	0	0	0	0	0	0	0	0	0	0	0	8	18	50	77
16	0	0	0	0	0	0	0	0	0	0	0	0	0	0	0	1	0	2	0	7	11
17	0	0	0	0	0	0	0	0	0	0	0	0	0	0	0	0	0	0	1	0	2
18	0	0	0	0	0	0	0	0	0	0	0	0	0	0	0	0	0	3	1	2	6
19	0	0	0	0	0	0	0	0	0	0	0	0	0	0	0	0	0	0	0	1	2
20	0	0	0	0	0	0	0	1	0	0	0	0	0	0	0	1	0	2	0	3	7
	100	0	99	97	96	1	4	44	76	91	83	58	92	2	93	96	96	93	97	90	

Table 3 Unstable sub-space projection matrix (see definition 3.1 in the text), for the two 24 h experiments expB1 and expC. The indices on the vertical axis refer to expB1 SVs, the indices on the horizontal top axis to expC SVs. Each element m_{ij} of the matrix M gives the squared scalar product between the i-th expB1 SV and the j-th expC SV. For each line, the last column gives the % of norm of each of the expB1 SVs that is explained by the first 20 expC SVs. For each column, the last line gives the analogous information for the expC SVs norms explained by the 24 h sub-space.

vertical structure of the SVs is more realistic, with a growth not confined to the lowest model levels as is the case for a large number of the expC SVs.

The comparison of expB1 and expB3 shows the importance of having turbulent transport and surface drag applied to the horizontal momentum equations. If compared with the control expA, the differences of the non-linear basic state evolution computed from expB3 are larger than the one from expB1, with values similar to those of expC. The presence of the surface drag in expB3 decreases the flow differences at the lowest model level with respect to expC, but the absence of momentum turbulent transport is clearly evident. If we compare the unstable sub-spaces, we can see that the similarity indices of the two experiments expB1-expB3 are almost as the expB1-expC:

Sub-space dimension N	ExpB1-ExpB3	ExpB1-ExpC
10	98%	97%
20	83%	74%

Looking in detail at the SVs, both expB3 and expC have SVs almost completely orthogonal to the expB1 unstable sub-space. The expB3 SVs have structures similar to the expC SVs, with perturbations confined in the lowest model levels, with the temperature field changing sign from one level to the other. From this we can conclude that the presence of the surface drag in expB3 prevents large unrealistic growth of the wind, in the first model level, but does not prevent the problem of the vertical structure of the SVs. A surface drag scheme needs to be coupled with a turbulent transport scheme to cure this problem.

The comparison between expB2 and expB1 shows the impact of the turbulent transport applied to the dry static energy, with no surface heat flux. Let us first consider the non-linear basic state evolution of expB2: the flow differences expB2-expA are larger than the expB1-expA ones. As already mentioned in section 2, the differences expB2-expA in the temperature fields have values similar to the differences expC-expA: at the two lowest model levels $\varepsilon(t=24h)$ reaches values of 261% and 176%, similar to expC. Nevertheless, the impact on the SVs is almost negligible: the similarity indices for $N=10, 20$, computed between expB3 and expB1, have values greater than 99%, indicating that including the turbulent transport of dry static energy does not induce any measurable change.

Some experiments have been run to test the impact of modifying the scheme parameters $u^*_{L,S}$, $z_{0_{L,S}}$, h_0: the sensitivity of the results when changing by a factor of 2 $u^*_{L,S}$, $z_{0_{L,S}}$, and with $700\ m \le h_0 \le 1500\ m$, was very small. The unstable sub-spaces of all these experiments were very similar.

The following conclusions can be drawn from the results presented in section 2 and 3:

- the simple vertical diffusion and surface drag scheme implemented seems to give reasonable results;
- the expB1 configuration, with the surface drag and the turbulent transport applied only to the horizontal momentum components, gives a non-linear basic state evolution very similar to the evolution computed using a version of the ECMWF scheme;
- the application of the turbulent transport to the dry static energy without a correct surface heat flux parametrization produces a poor non-linear basic state time evolution;
- the parametrization of the surface drag and the turbulent transport in the horizontal momentum equations is essential to prevent very fast growing structures unrealistically confined in the lowest model levels;
- the impact of applying the turbulent transport to the dry static energy on the unstable sub-space definition, is negligible.

4. SVs SENSITIVITY TO THE TRAJECTORY COMPUTATION

The basic state evolution is computed using a non-linear model, whose equations are an approximation of the processes of the real atmosphere. The tangent model equations are defined as the linearization of the non-linear equations around a time evolving trajectory. These tangent equations can be defined to be the first order term of the Taylor expansions of the non-linear equations, computed for a small perturbation. Since both the non-linear and the tangent models are approximations, we need not to assume that the tangent model is a precise first order approximation of the non-linear model. So, to have a more complete non-linear model to compute the basic state evolution, we can allow the non-linear model to use the full physics parametrization, and the tangent model to use the tangent version of the simplified scheme. Experiments run with the same tangent model, but different non-linear models are shown in this section.

Two more experiments have been run to study the impact on the unstable sub-space definition, of the way the trajectory is computed. Experiment expD1 has been run with an optimization time interval of 24 hours, with a basic state evolution computed using the ECMWF version of the vertical diffusion and surface drag scheme, while the tangent and the adjoint versions of the model have been run using the tangent and the adjoint version of the simple scheme. ExpD2 has been run in the same configuration, but with an optimization time interval of 48 hours. ExpD1 has been compared with expB1, and expD2 with an analogous experiment with an optimisation time interval of 48 h, run in the same configuration as expB1.

The two unstable sub-spaces generated by the SVs of the two 24 h experiments are very similar, the similarity indices for N=10, 20, computed between expB1 and expD1, having values of almost 100%. The similarity indices computed between the 48 h experiments have the same values. This result indicates that

it can be feasible to apply the adjoint technique with a tangent version that is not the exact first order approximation of the non-linear model.

5. SVs SENSITIVITY TO OPTIMIZATION TIME INTERVAL

Experiments were performed to study the impact of the optimisation time interval (hereafter OTI), on the definition of the unstable sub-spaces, with four different starting dates: 17.01.91, already described, and 17.01.90, 17.01.91, 19.02.91. All these situations are characterized by a regime transition from a situation of blocked flow to a more zonal type flow.

All the SV computations were run with the configuration of expB1, with surface drag and turbulent transport applied only to the horizontal momentum equations. Unstable sub-spaces have been computed with an OTI of 12, 24, 36, 48, 60 and 72 hours. The comparison of the projection matrices, and the analysis of the similarity indices can indicate how well the unstable sub-space computed with a OTI approximate the unstable sub-space with different OTIs.

Looking at the amplification factor curves of the different situations, we can classify the situations from the most unstable to the least unstable, looking at the amplification factor of the fastest growing perturbations. The 17.01.89 and the 17.01.90 can be classified as the most unstable, the 17.01.91 slightly less unstable, and the 19.02.91 as the least unstable situation of the four. If we consider for example the leading amplification factor for a 36 h OTI, we have respectively 8.7 for the 17.01.89, 9.3 for the 17.01.90, 8.0 for the 17.01.91 and 6.9 for the 19.02.91.

Let us first analyze the results of the experiments run with starting date 17.01.89. Fig. 5 shows the amplification factors of the SVs of these experiments (the results of the experiment run with 60 h OTI has been omitted for clarity). Fig. 5 clearly shows that increasing the OTI, a better separation of the SVs based on their growth can be achieved. The first 10-20 SVs of experiments run with an OTI greater than 36 hours are characterized by a faster growth rate that distinguishes them from the rest of the unstable spectrum. This is still evident for the experiment run with a 24 h OTI, but it is not valid for the experiment with an OTI of 12 h. Increasing the OTI, the e-folding time decreases: the e-folding time of the first SVs of the 12 h OTI experiment is half of the e-folding time of the 72 h OTI SVs.

Tables 4 and 5 show the similarity indices computed between the different experiments, for the first N SVs, where N=10, 20. If we consider each table as a matrix S^N, its element is defined as (see eq. 17):

$$s^N_{ij} = s\,(t_i, t_j; N) \tag{18}$$

Each element s^N_{ij} indicates how well the unstable sub-space generated by the first N SVs of the experiment

Table 4

N=10	12	24	36	48	60	72
12	--	31	13	7	5	4
24	31	--	69	42	30	23
36	13	69	--	74	54	41
48	7	42	72	--	87	68
60	5	29	54	87	--	88
72	4	23	41	68	88	--

Table 4 Similarity index matrix relative to the 17.01.89 (see definition 5.1 in the text): the unstable sub-spaces generated by the first 10 SVs of the experiments performed with a different optimisation time interval are compared.

Table 5

N=20	12	24	36	48	60	72
12	--	34	13	7	5	4
24	34	--	63	38	24	19
36	13	63	--	80	54	40
48	7	38	81	--	82	62
60	5	24	54	82	--	86
72	4	19	40	62	86	--

Table 5 As table 4, but for the unstable sub-spaces generated by the first 20 SVs.

Table 6

N=10	12	24	36	48	60	72
12	--	28/5	9/4	5/3	4/2	3/1
24	28/5	--	59/12	32/9	21/7	16/4
36	9/4	59/12	--	70/7	46/9	34/6
48	5/3	21/7	46/9	--	79/8	60/5
60	4/2	21/7	46/9	79/8	--	82/4
72	3/1	17/5	34/6	60/5	82/5	--

Table 6 Mean similarity indices and standard deviations, computed from the similarity matrices of the 4 situations described in the text, for the unstable sub-spaces generated by the first 10 SVs. The first value of each element of the matrix is the similarity index, while the second value after the "/" is the standard deviation. For example, the mean similarity index and the standard deviation of the experiments run with 24 h and 36 h optimisation time intervals, are respectively 59 and 12.

Table 7

N=20	12	24	36	48	60	72
12	--	31/5	11/3	5/2	4/2	3/1
24	31/3	--	59/2	34/3	23/2	18/1
36	11/3	59/2	--	77/3	52/2	38/1
48	5/2	34/3	77/3	--	82/1	61/1
60	4/2	23/2	52/2	82/1	--	83/1
72	3/1	17/1	39/1	61/1	83/1	--

Table 7 As table 6, but for the unstable sub-spaces generated by the first 20 SVs.

run with OTI equal to t_i, can be constructed from a linear combination of the first N SVs of the experiment run with OTI equal to t_j. Since the elements of each unstable sub-space span only a sub-space of the phase space of the system, this matrix is not symmetric.

Several considerations can be drawn from these two tables:

5a) The values of S^{10} are higher or equal to the S^{20} values for OTI greater than 36 h. This indicates that the first 10 most unstable directions remain more similar than the first 20. The leading growing perturbations are less sensitive to the OTI definition.

5b) Consider two experiments with OTI equal to t_i and to $t_i + \Delta$. The results of tables 4 and 5 show that, if

$$t_i > t_j$$

then

$$s\,(t_i,t_i+\Delta;N) > s\,(t_j,t_j+\Delta;N) \qquad (19)$$

The analysis of the elements of the two matrices can give an indication of the time range Δ, for which the unstable sub-space of an experiment with an OTI equal to t_i, can approximate the unstable sub-spaces of the experiments with an OTI t_j in the range $t_i - \Delta \le t_j \le t_i + \Delta$. If we consider a threshold of 60%, table 4 shows that the experiment with a 48 h OTI sub-space can give an acceptable approximation of the unstable sub-space with N=10 of the experiments with OTIs equal to 36 h, 60 h and 72 h. Note that the range Δ decreases with the OTI.

5c) The sub-space generated by the SVs computed with a 12 h OTI seems to distinguish itself from all the others, since all the values $s\,(t_i$=12,$t_j;N)$ are very small. On the contrary, the unstable sub-spaces generated by the SVs computed with an OTI greater than 36 h are very similar one to the other.

The comparison of the unstable sub-spaces has been done for the other three situations. Tables 6 and 7 show the mean similarity index, and the standard deviation computed using the results of all the 4 situations. The first general consideration that can be drawn from the comparison of table 7 with table 6 is that the similarity indices with N=20 are characterized by higher values and smaller standard deviation. This contradicts consideration 5a. Moreover, the fact that the standard deviations for N=20 are smaller that the standard deviations for N=10, shows that the leading fastest growing perturbations depend more on the

situation than the definition of the unstable sub-space generated by the first 20 SVs. The smaller the unstable sub-space dimension, the more its definition depends on the situation.

A detailed analysis of the similarity indices for the different situations seems to show a relation between the instability of the situation and the similarity between the different unstable sub-spaces. The definition of the fastest growing directions is less influenced by the choice of the OTI for a more unstable situation like the 17.01.89, than for a more stable situation like the 19.02.91. In fact the similarity indices computed for the 17.01.89 are higher than the values of the 19.02.91.

Consideration 5b is confirmed by tables 6 and 7, although the definition of the time range Δ is a function of the situations. Consideration 5c is also confirmed. The fact that the unstable sub-space generated with a 12 h OTI is so different from the others can be related to the poor separation of the SVs that can be achieved with a 12 h time interval. A 24 h interval seems to be the minimum time interval necessary to clearly identify in the spectrum of the unstable perturbations directions with a much faster growth than the others. This is clearly shown by Fig. 5.

To give an idea of the SV structures, Fig. 6a shows the first 6 SVs computed for the 17.01.89, with the configuration of expB1, with a 36 h OTI (streamfunction, at model level 11, that is almost 500 hPa). Each SV has been normalized to have a unit energy norm. The first 6 SVs are very localized. They are characterized by a barotropically and baroclinically unstable pattern, with a westward tilt with height, and a horizontal pattern which extract energy from the basic state. The first two SVs have maximum amplitude over western Pacific with maximum amplitude around model level 13, that is around 600 hPa (see Fig. 7a and 7b), where the mid-latitude jet has a region of maximum amplitude. The 3rd and the 4th are localized over north-eastern North America, western Atlantic, with maximum amplitude localized in the vertical as it is the case of the leading two SVs.

Fig. 6b shows their final state when linearly integrated. The same model levels have been plotted, with a contour interval 4 times greater. All of them grow very fast and propagate eastward, changing their shape from an initial structure horizontally curved to gain energy from the basic state, to a structure that gives energy to the basic state.

Fig. 7 shows the time evolution of the energy, computed at each model level. The figure shows the region of maximum growth of each SV, and clearly illustrates how the presence of the vertical diffusion and surface drag scheme prevents the presence of growing structures close to the surface.

6. CONCLUSIONS

The adjoint technique has been applied to the computation of the fastest growing perturbations of a primitive equation model. A simple scheme has been implemented in the non-linear, the tangent and the adjoint version of a primitive equation model. Experiments have been performed to study the impact of the scheme on the non-linear evolution of the basic state, and on the definition of the unstable sub-space of the system, i.e. the sub-space generated by the first N SVs. A similarity index has been defined to compare two different sub-spaces.

We have shown that the non-linear evolution computed using the simple scheme is similar to the evolution computed using a version of the operational ECMWF scheme. The sensitivity of the non-linear evolution to the tuning parameters of the scheme is very small. The sensitivity of the unstable sub-space definition to the tuning parameters is also very small. These results indicate that the IFS system with the simple physics is now capable of giving realistic results, without having growing structures unrealistically confined to the first model levels (their time evolution must be similar to an error field evolution).

One of the goals of this work was to study the sensitivity of the SVs to the optimisation time interval. In section 5 we compared the unstable sub-spaces generated with optimisation time intervals ranging from 12 to 72 h, for 4 different situations. The tangent propagator, and its adjoint, are a function of the time interval, and so we expect the sub-spaces generated with different optimisation time intervals to be different. However, since the unstable directions are related to the atmospheric flow characteristic, we also expect that the unstable sub-spaces do not depend too strongly on the choice of the optimization time interval.

The results show that the unstable sub-spaces of each situation, generated with time intervals longer then 24 h, are similar one to each other, while the sub-space generated with a 12 h optimisation time interval is very different from all of the others. The similarity between sub-spaces generated with different optimisation time intervals increases with the optimisation time interval. The subspace generated using an optimization time interval t_i, for a very unstable situations, can give an accurate approximation of the sub-spaces with an optimisation time interval $t_i - \Delta \leq t_j \leq t_i + \Delta$, where the range Δ depends on t_i.

The similarity between unstable sub-spaces depends on the situations: more unstable situations, like the situation of the 17.01.89, seems to have SVs less sensitive to the optimisation time interval definition.

The second focus of this work was to study the impact on the SVs of the way the non-linear basic state evolution is computed. It has been shown that it is possible to work in a framework where the non-linear model has a complex vertical diffusion scheme, but the tangent version has a more simple scheme. In the

case of surface drag and vertical turbulent transport, it has been shown that the impact is almost negligible, the SVs computed using different trajectories being very similar.

ACKNOWLEDGMENTS

I would like to thank A Beljaars and P Courtier for very useful discussions we had during the development of the simple physics scheme.

REFERENCES

Buizza, R., J. Tribbia, F. Molteni, T. Palmer, 1992: "Computation of Optimal Unstable Structures for a Numerical Weather Prediction Model", submitted to Tellus A.

Buizza, R., 1992: "Unstable perturbations computed using the adjoint technique", RD Tech.Mem. No. 189, ECMWF.

ECMWF Research Manual 3, 1991: "ECMWF forecast model: Physical Parametrization".

Lacarra, J.-F. and O. Talagrand, 1988: "Short range evolution of small perturbations in a barotropic model", Tellus, 40A, 81-95.

Lorenz, E.N., 1965: "A study of the predictability of a 28-variable atmospheric model", Tellus XVII, 3, 321-333.

Molteni, F. and T.N. Palmer, 1992: "Predictability and finite-time instability of the northern winter circulation", submitted to QJRMS.

Mureau, R., F. Molteni and T.N. Palmer, 1992: "Ensemble prediction using dynamically-conditioned perturbations", submitted to QJRMS.

Rabier, F. and P. Courtier, 1991: "Four-dimensional assimilation in the presence of baroclinic instability", RD Tech.Mem. No. 183, ECMWF.

Simon, H.D., 1984: "The Lanczos algorithm with partial re-orthogonalization", Math.Comp., 42, 165, 115-142.

Strang, G., 1986: "Introduction to applied mathematics", Wellesley-Cambridge Press.

Troen, I. and L. Mahrt, 1986: "A simple model of the atmospheric boundary layer; sensitivity to surface evaporation", Bound.Layer Meteor., 37, 129-148.

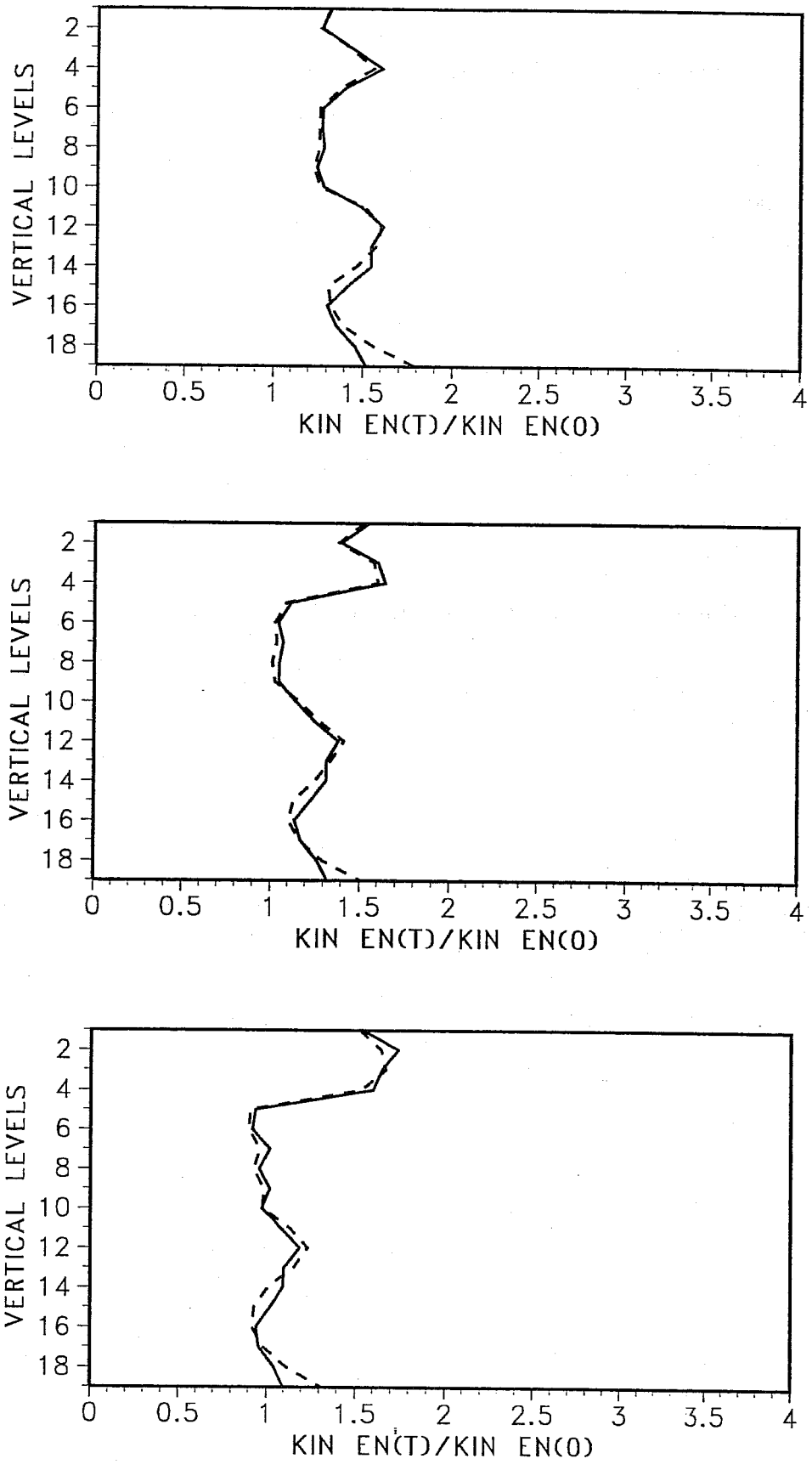

Fig. 1 Vertical cross section of the ratio between the kinetic energy at forecast time t and the initial value, for expB1 (solid line) and expA (dashed line): 1a refers to 24 h, 1b to 48 h and 1c to 72 h.

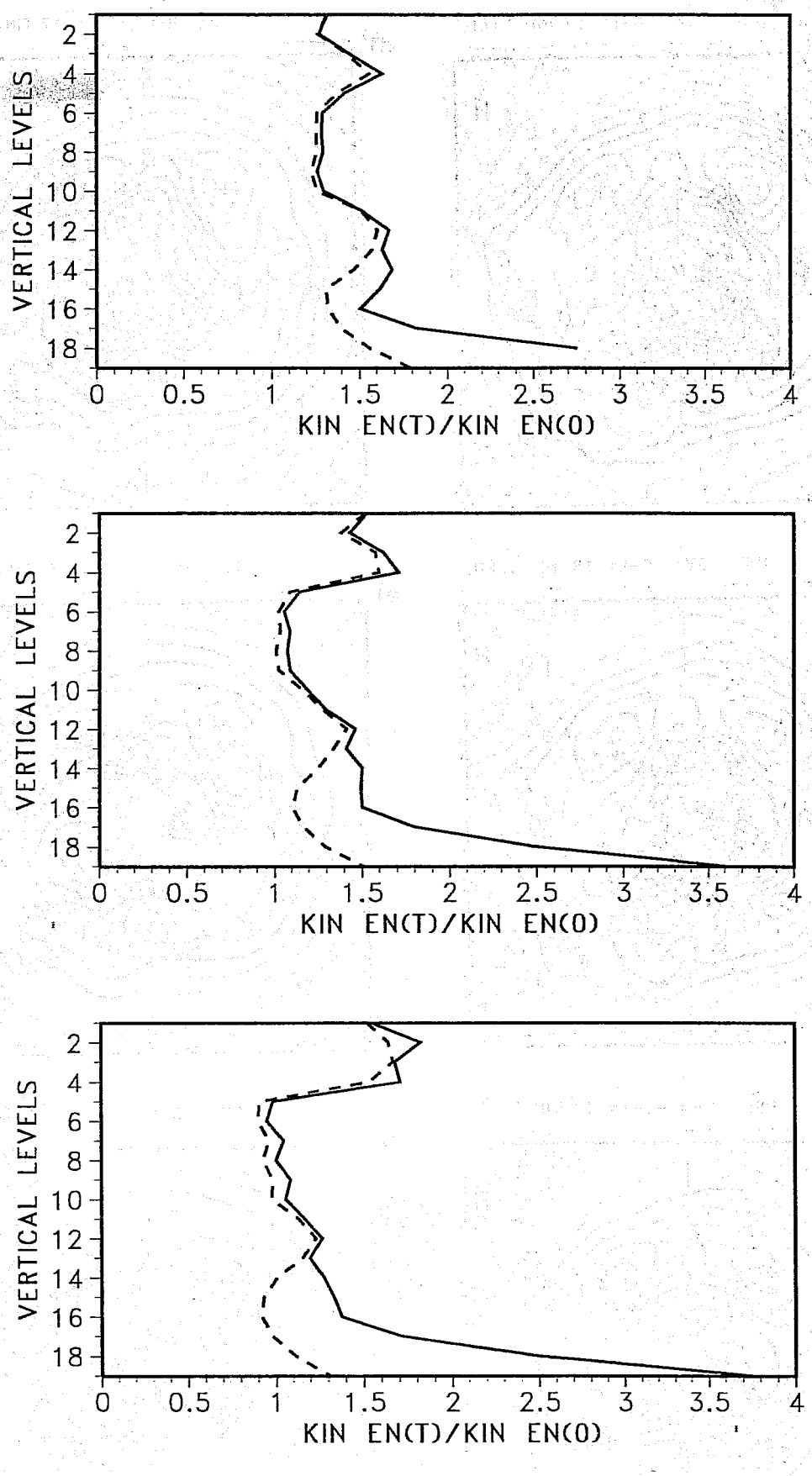

Fig. 2 Same as Fig. 1, but for expC (solid line) and expA (dashed line).

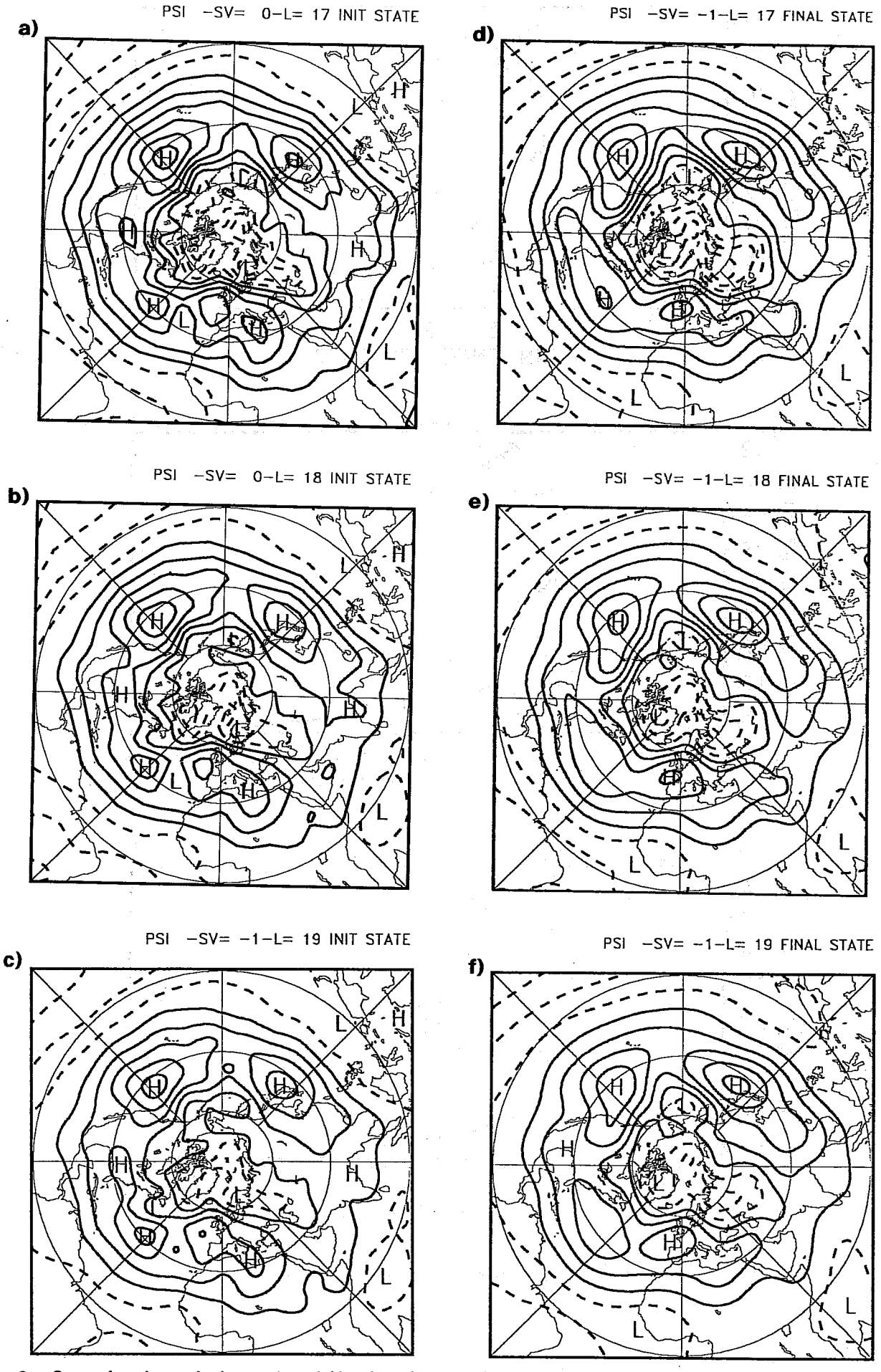

Fig. 3 Streamfunction at the lowest 3 model levels at the initial time (Fig. 3a, 3b and 3c), and after 24 h non-linear time evolution (Fig. 3d, 3e and 3f) computed by expA. Contour intervals every 0.5.

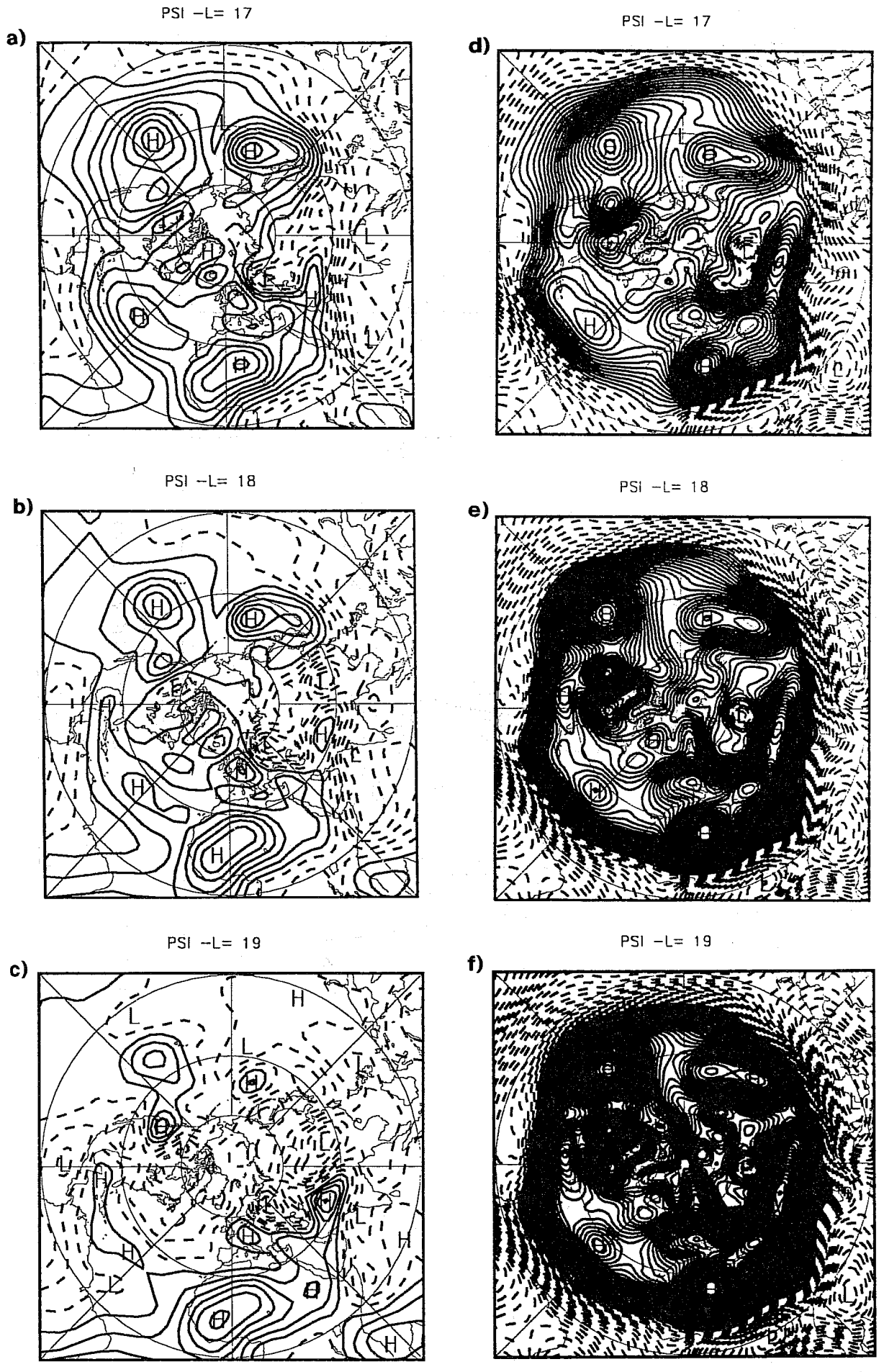

Fig. 4 Difference field of the 24 h forecast streamfunction, at the lowest 3 model levels, between expB1 and expA (Fig. 4a, 4b and 4c), and between expC and expA (Fig. 4d, 4e and 4f). The contour interval is the same as Fig. 3.

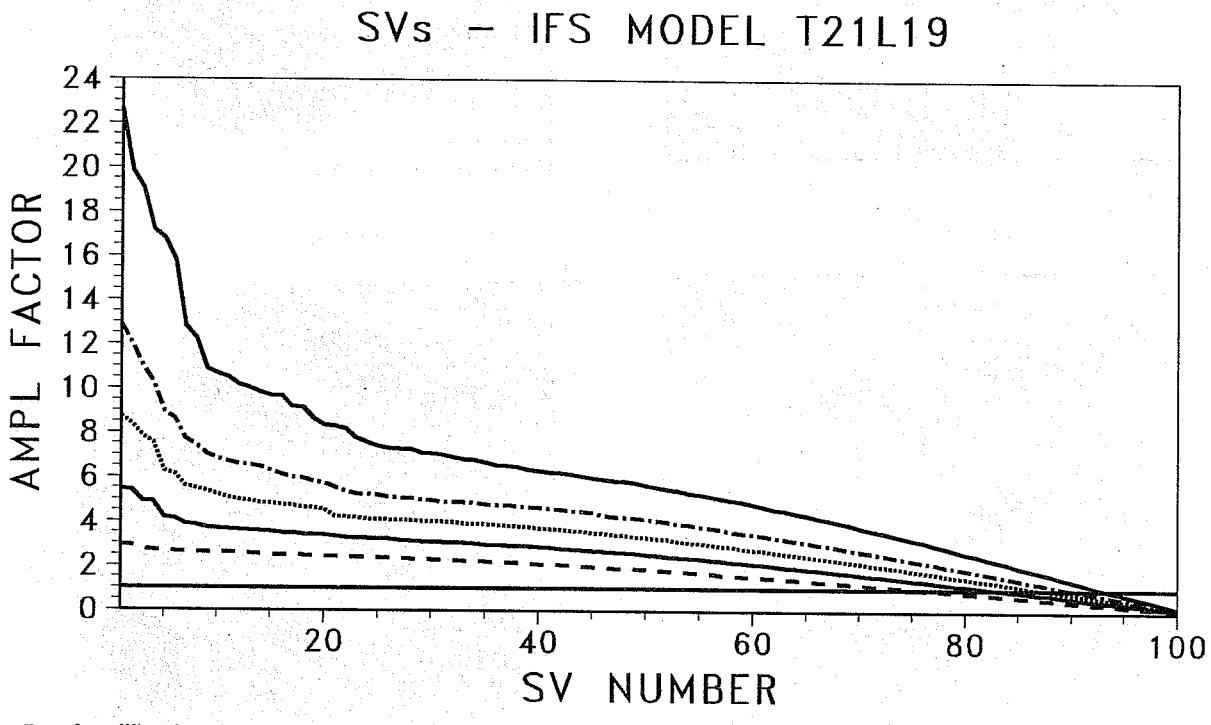

Fig. 5 Amplification factors of the SVs computed with different optimisation time intervals, for the situation of the 17.01.89: dashed line 12 h, middle solid line 24 h, dotted line 36 h, chain dashed line 48 h, upper solid line 72 h.

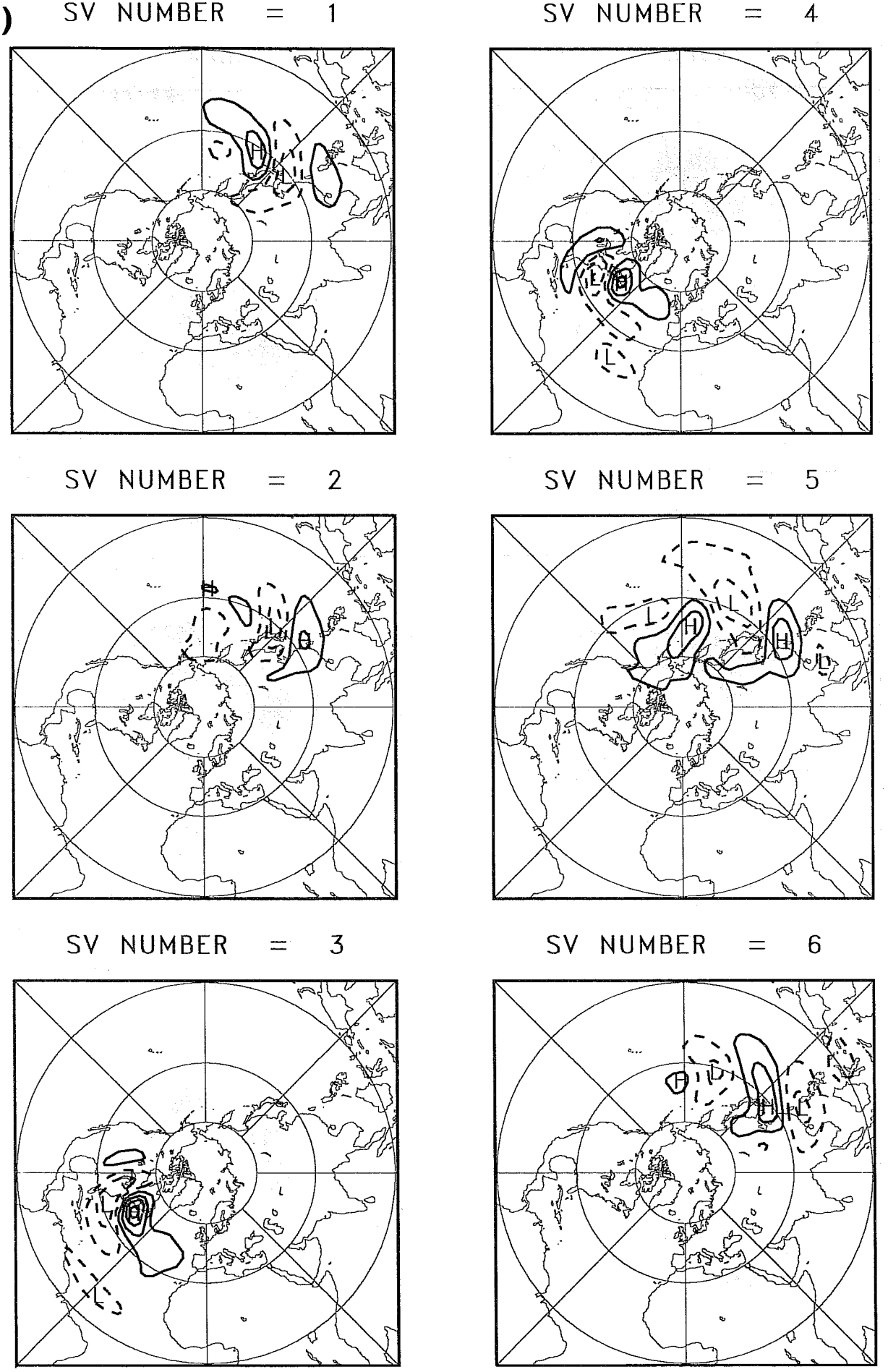

Fig. 6 First 6 36 h SVs relative to the 17.01.89, computed with an optimisation time interval of 36 h. The streamfunction at model level 11 (approximately 500 hPa) of the normalized SVs, with total unity energy norm, is plotted. Fig. 6a shows their structure at time t_0, and Fig. 6b their structure after 36 h of tangent evolution. The contour interval of Fig. 6a is 0.005, of Fig. 6b is 4 times greater, 0.02.

b)

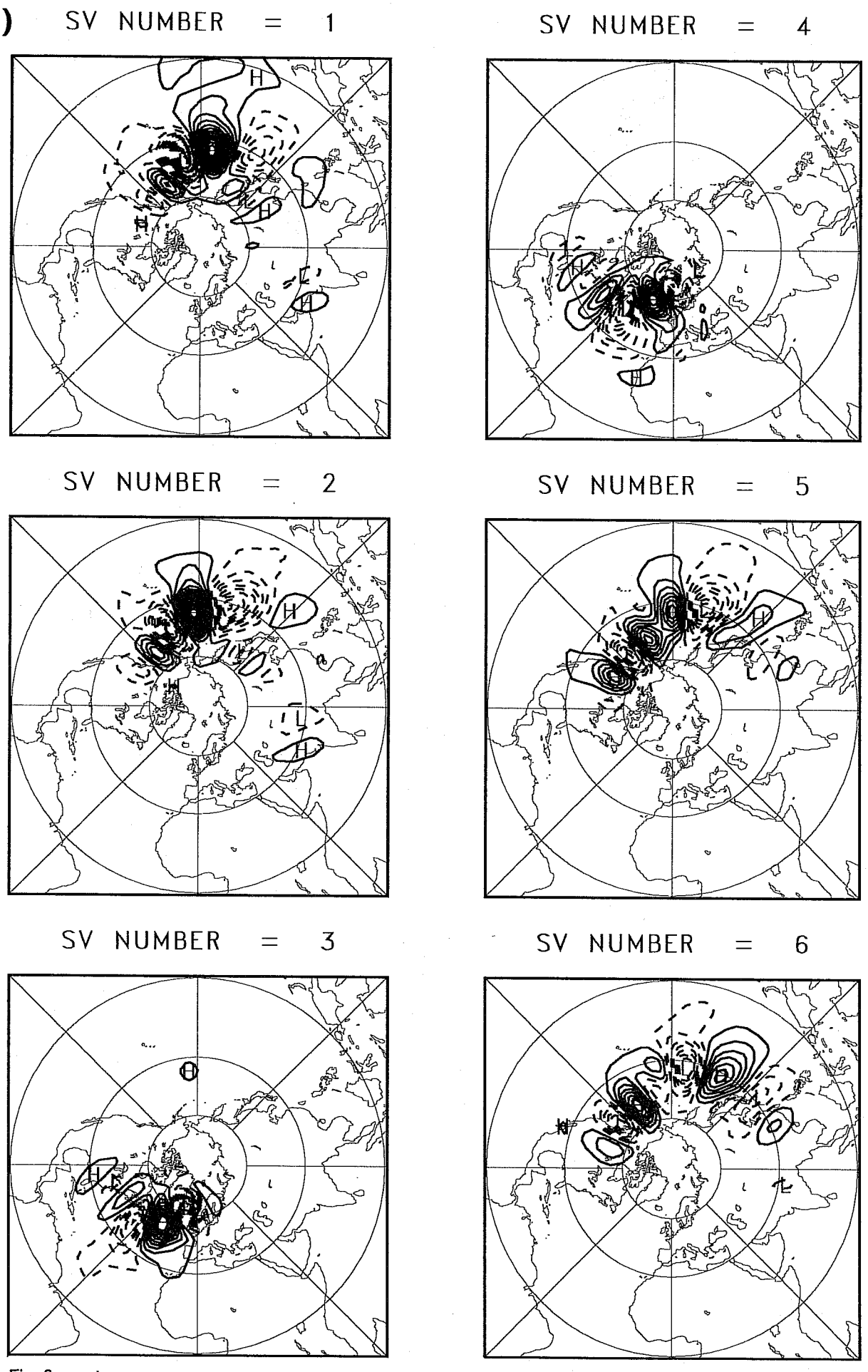
SV NUMBER = 1
SV NUMBER = 4
SV NUMBER = 2
SV NUMBER = 5
SV NUMBER = 3
SV NUMBER = 6

Fig. 6 cont

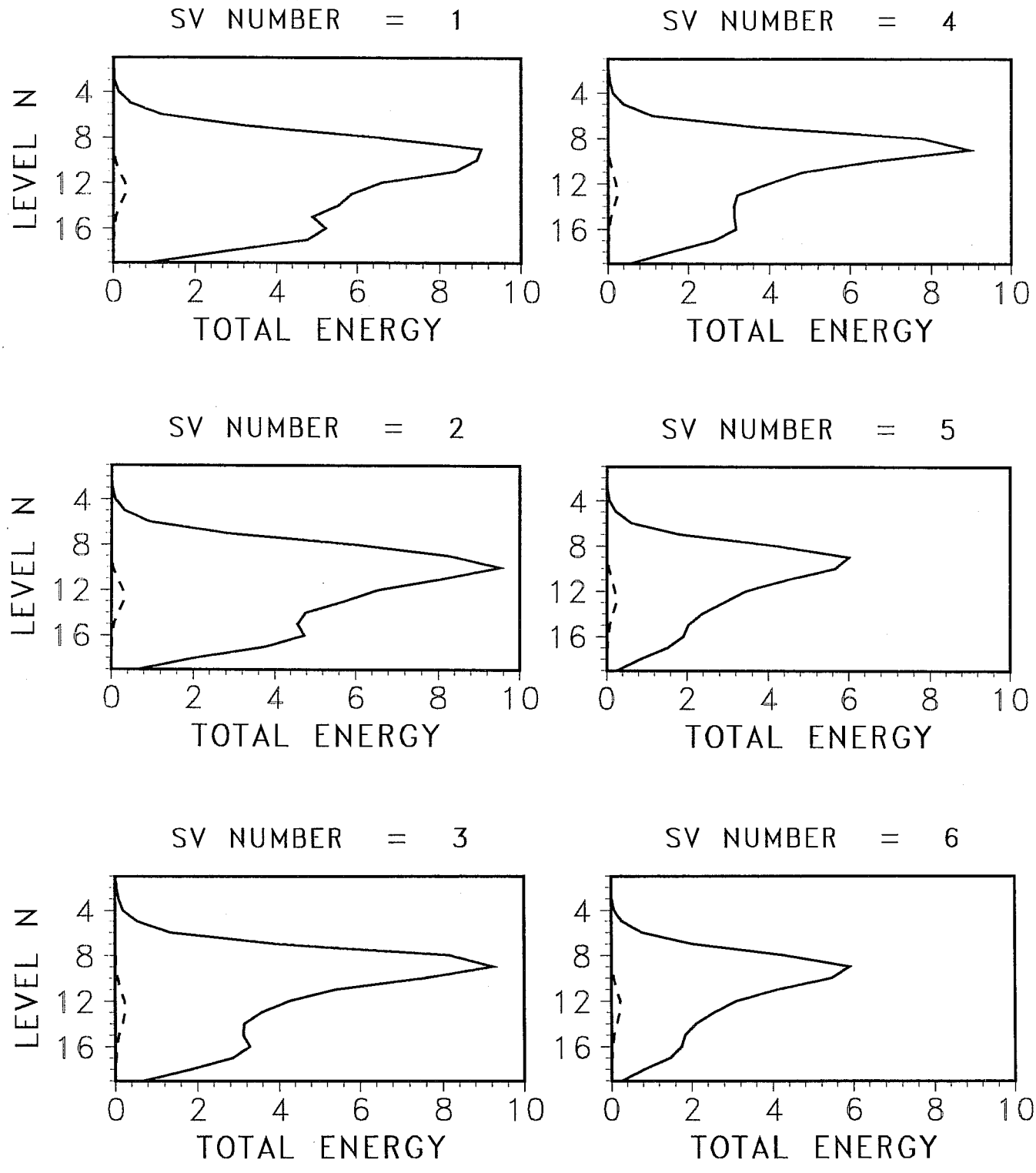

Fig. 7 Vertical cross section of the total energy, of the first 6 36 h SVs of the 17.01.89, shown in Fig. 6: the dashed line is the initial value, the solid line is the energy after 36 h tangent evolution.